Optimized Intermolecular Potential Functions for Liquid Hydrocarbons

William L. Jorgensen,* Jeffry D. Madura, and Carol J. Swenson

Contribution from the Department of Chemistry, Purdue University, West Lafayette, Indiana 47907. *Received March 12, 1984*

Abstract: Optimized intermolecular potential functions have been determined for hydrocarbons through Monte Carlo simulations of 15 liquids: methane, ethane, propane, *n*-butane, isobutane, *n*-pentane, isopentane, neopentane, cyclopentane, *n*-hexane, 1-butene, *cis*- and *trans*-2-butene, isobutene, and benzene. To achieve high accuracy, 12 unique group types were identified and their associated Lennard-Jones parameters were established. The average deviation from experiment for the computed densities and heats of vaporization is 2% and trends for isomeric series are reproduced. Conformational results were also obtained for five liquids and revealed no condensed-phase effects on the conformer populations. Structural analyses focus on trends as a function of chain length and branching of the monomers.

Introduction

The structure and behavior of complex organic and biochemical systems may be examined at the molecular level using molecular dynamics and statistical mechanics techniques. Though the progress in this area has been great during the last decade,[1-4] increased accuracy and success of the methods depends critically on the development of improved intermolecular potential functions (IPFS) for describing the interactions between components in the systems. Traditionally, crystal data have provided a basis for parameterization of such functions for hydrocarbons and protein constituents.[5-12] However, a primary target of the simulations is not solids, but rather solutions of organic and biochemical substrates near 25 °C. Consequently, it is particularly appropriate to develop IPFS that can reproduce experimental data on fluids. This is relatively costly in comparison to the crystal calculations since it requires numerous molecular dynamics or Monte Carlo simulations with trial sets of parameters. So far, the procedure has primarily been applied to water by Stillinger and Rahman and by our group.[13,14] We are now engaged in extending the treatment to a variety of organic liquids. The first systems to be addressed were the liquid hydrocarbons including alkanes and alkenes, as described here.

The aim is to develop IPFS that may be rapidly evaluated in fluid simulations and that yield accurate thermodynamic and structural results for liquids. To achieve this goal, Monte Carlo simulations have been carried out for 15 hydrocarbon liquids: methane, ethane, propane, *n*-butane, isobutane, *n*-pentane, isopentane, neopentane, cyclopentane, *n*-hexane, 1-butene, *cis*- and *trans*-2-butene, isobutene, and benzene. Twelve constituent groups were identified and corresponding Lennard-Jones parameters were optimized. The key points of comparison with experiment are for the energies and densities of the liquids which are reproduced with average errors of 2%. Such accuracy cannot be expected for liquids from IPFS based on crystal data and that use many fewer group types.

Besides determination of the optimized IPFS, the present simulations also provide extensive structural and conformational results for the hydrocarbon liquids. Trends as a function of chain length and branching are considered. Such a comprehensive treatment has not been reported previously since among these liquids only methane,[15] ethane,[16] *n*-butane,[17,18] and benzene[19] have been the subjects of prior simulations.

Table I. Standard Geometrical Parameters for Hydrocarbons[a]

bond lengths (Å)		bond angles (deg)	
C4–C4	1.53	C–C4–C	112.0
C4–C3	1.50	C–C3–C	124.0
C3 = C3	1.34		
C3 – C3[b]	1.40		

[a] C4 and C3 are sp^3 and sp^2 carbons, respectively. [b] Aromatic CC bond.

Computational Methods

(a) Intermolecular Potential Functions. In previous work, we reported a set of simple, transferable intermolecular potential functions (TIPS) for water, alkanes, alcohols, and ethers.[20] The parameters were obtained primarily by fitting to gas-phase data on dimers and tested in Monte Carlo simulations of liquid water, *n*-butane, methanol, ethanol, and several ethers.[17,20,21] The functions yield average errors of 5–10% for the densities and energies of these liquids, but have not been tested for branched systems. The form of the TIPS has been retained in the present work; however, it became apparent quickly that reparameterization would be necessary to treat branched alkanes accurately.

To avoid confusion with the TIPS, the present potential functions along with the TIP4P potential for water[14] will be referred to as the OPLS functions for optimized potentials for liquid simulations. For these functions, molecules are represented by interaction sites usually located on the nuclei. The interaction energy between two monomers a and b is then determined by

(1) McCammon, J. A.; Karplus, M. *Acc. Chem. Res.* **1983**, *16*, 187.
(2) Nemethy, G.; Pear, W. J.; Scheraga, H. A. *Annu. Rev. Biophys. Bioeng.* **1981**, *10*, 459.
(3) Dauber, P.; Hagler, A. T. *Acc. Chem. Res.* **1980**, *13*, 105.
(4) Jorgensen, W. L. *J. Phys. Chem.* **1983**, *87*, 5304.
(5) Kitaigorodskii, A. I. "Molecular Crystals and Molecules"; Academic Press: New York, 1973.
(6) Williams, D. E. *J. Chem.Phys.* **1965**, *43*, 4424; **1967**, *47*, 4680.
(7) Warshel, A.; Lifson, S. *J. Chem. Phys.* **1970**, *53*, 582.
(8) Momany, F. A.; McQuire, R. F.; Burgess, A. W.; Scheraga, H. A. *J. Phys. Chem.* **1975**, *79*, 2361.
(9) Dunfield, L. G.; Burgess, A. W.; Scheraga, H. A. *J. Phys. Chem.* **1978**, *82*, 2609.
(10) Snir, J.; Nemenoff, R. A.; Scheraga, H. A. *J. Phys. Chem.* **1978**, *82*, 2497, 2527.
(11) Gelin, B. R.; Karplus, M. *Biochemistry* **1979**, *18*, 1256.
(12) Lifson, S.; Hagler, A. T.; Dauber, P. *J. Am. Chem. Soc.* **1979**, *101*, 5111.
(13) Stillinger, F. H.; Rahman, A. *J. Chem. Phys.* **1974**, *60*, 1545; **1978**, *68*, 666.
(14) Jorgensen, W. L.; Chandrasekhar, J.; Madura, J. D.; Impey, R. W.; Klein, M. L. *J. Chem. Phys.* **1983**, *79*, 926.
(15) Verlet, L.; Weis, J.-J. *Mol. Phys.* **1972**, *24*, 1013.
(16) Byrnes, J. M.; Sandler, S. I. *J. Chem. Phys.* **1984**, *80*, 881.
(17) (a) Jorgensen, W. L.; Binning, R. C.; Bigot, B. *J. Am. Chem. Soc.* **1981**, *103*, 4393. (b) Jorgensen, W. L. *Ibid.* **1981**, *103*, 4721. (c) Jorgensen, W. L. *J. Chem. Phys.* **1982**, *77*, 5757.
(18) (a) Ryckaert, J.-P.; Bellemans, A. *Discuss. Faraday Soc.* **1978**, *66*, 95. (b) Weber, T. A. *J. Chem. Phys.* **1978**, *69*, 2347.
(19) (a) Evans, D. J.; Watts, R. O. *Mol. Phys.* **1976**, *32*, 93. (b) Claessens, M.; Ferrario, M.; Ryckaert, J.-P. *Ibid.* **1983**, *50*, 217. (c) Linse, P. *J. Am. Chem. Soc.* **1984**, *106*, 5425.
(20) Jorgensen, W. L. *J. Am. Chem. Soc.* **1981**, *103*, 335, 341, 345.
(21) (a) Jorgensen, W. L.; Ibrahim, M. *J. Am. Chem. Soc.* **1981**, *103*, 3976. (b) Chandrasekhar, J.; Jorgensen, W. L. *J. Chem. Phys.* **1983**, *77*, 5073.

0002-7863/84/1506-6638$01.50/0

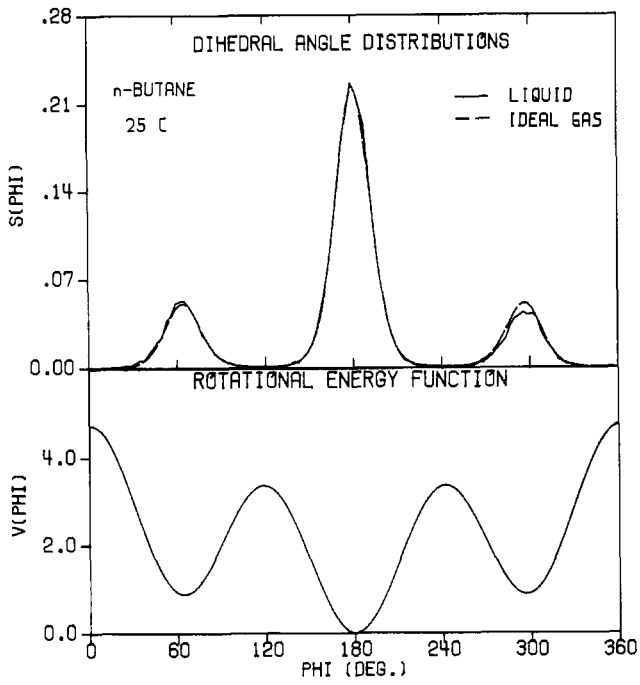

Figure 1. Bottom: potential function (kcal/mol) for rotation about the central CC bond in *n*-butane. Top: population distributions for the dihedral angle. Units for $s(\phi)$ are mole fraction per degree $\times 10^{-3}$.

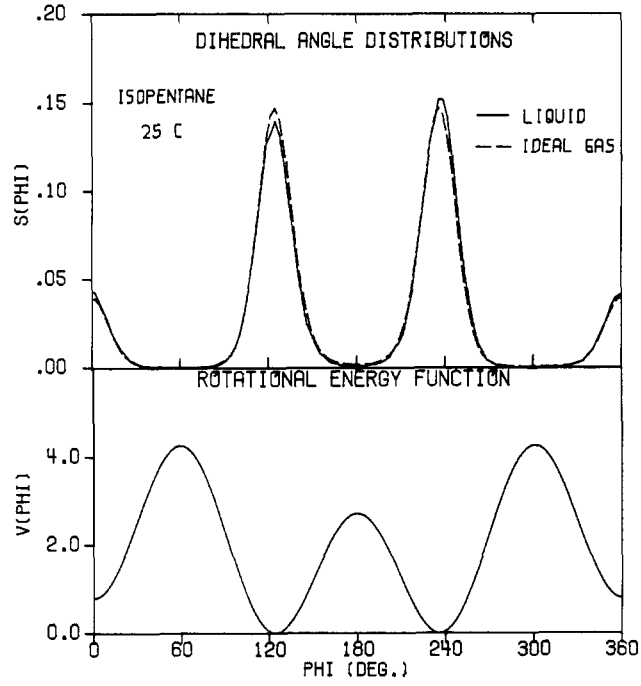

Figure 2. Bottom: potential function (kcal/mol) for rotation about the central CC bond in isopentane. Top: computed population distributions for the dihedral angle. Units as in Figure 1.

Coulomb and Lennard-Jones interactions between all intermolecular pairs of sites (eq 1). Standard combining rules are used,

$$\epsilon_{ab} = \sum_{i}^{\text{on } a} \sum_{j}^{\text{on } b} (q_i q_j e^2/r_{ij} + A_{ij}/r_{ij}^{12} - C_{ij}/r_{ij}^{6}) \qquad (1)$$

i.e., $A_{ij} = (A_{ii}A_{jj})^{1/2}$ and $C_{ij} = (C_{ii}C_{jj})^{1/2}$. The A and C parameters may also be expressed in terms of Lennard-Jones ϵ's and σ's as $A_{ii} = 4\epsilon_i\sigma_i^{12}$ and $C_{ii} = 4\epsilon_i\sigma_i^{6}$.

Several more details must be noted. First, hydrogens on carbon are implicit while those on heteroatoms are explicitly retained. This united atom approximation was found to be acceptable in simulations of liquid methanol[20] and in the UNICEPP force field for polypeptides,[9] though earlier IPFS for hydrocarbons and proteins retain all hydrogens.[5-8] The use of implicit hydrogens is computationally highly advantageous and must be thoroughly considered.

Secondly, the interaction sites for the CH_n groups are centered on the carbons. Standard bond lengths and angles based on microwave results are assumed as summarized in Table I. However, torsional motions are included as described in the next section.

Finally, the CH_n groups in hydrocarbons are all taken as neutral ($q_i = 0$). This is supported by ab initio calculations on *n*-alkanes[4] and the lack of a dipole moment for gauche *n*-butane.[22] However, isobutane does have a dipole moment of about 0.1 D.[23] On the basis of the present results, the concomitant electrostatic effects are negligible or can be approximately absorbed in the Lennard-Jones terms.

(b) Intramolecular Potential Functions. Although the bond lengths and angles are fixed, internal rotations of the monomers are included in the simulations. A review of this topic has recently appeared and can be consulted for details on the implementation.[4] For molecules with a single internal rotational degree of freedom and C_s symmetry for one conformer, the Fourier series in eq 2

$$V(\phi) = V_0 + \tfrac{1}{2}V_1(1 + \cos\phi) + \tfrac{1}{2}V_2(1 - \cos 2\phi) + \tfrac{1}{2}V_3(1 + \cos 3\phi) \qquad (2)$$

suffices to describe the rotational potential energy. This is the case for *n*-butane, isopentane, and 1-butene. In these instances, we have determined the Fourier coefficients by fitting to the rotational potentials obtained from MM2 molecular mechanics

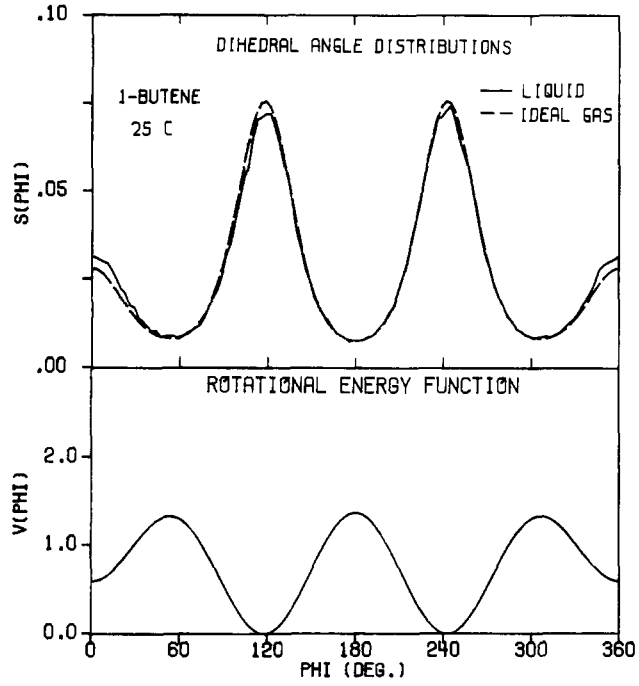

Figure 3. Bottom: potential function (kcal/mol) for rotation about the central CC bond in 1-butene. Top: computed population distributions for the dihedral angle. Units as in Figure 1.

Table II. Fourier Coefficients for Intramolecular Rotational Potential Functions[a]

molecule	V_0	V_1	V_2	V_3
1-butene	1.363	0.343	−0.436	−1.121
isopentane	2.713	1.526	0.533	−3.453
n-butane	0.0	1.522	−0.315	3.207
other *n*-alkanes	0.0	1.411	−0.271	3.145

[a] Units for the V's are kcal/mol.

(22) Durig, J. R.; Compton, D. A. C. *J. Phys. Chem.* **1979**, *83*, 265.
(23) Lide, D. R.; Mann, D. E. *J. Chem. Phys.* **1958**, *29*, 914.

calculations.[24] The rotational potentials for the three molecules are shown in the bottom halves of Figures 1–3 and the Fourier coefficients are recorded in Table II.

The $V(\phi)$ for *n*-butane has been used and discussed previously.[4,17c] The gauche-trans energy difference of 0.88 kcal/mol is in accord with experimental estimates for the gas phase.[4]

For isopentane, the doubly gauche conformer I has been defined

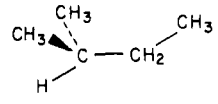

I

as $\phi = 0°$. The two mirror image trans minima then occur at about ±120°. The gauche-trans energy difference of 0.79 kcal/mol agrees with the Raman value of 0.81 ± 0.05.[25a]

The syn form (0°) of 1-butene is an energy minimum along with the two skew rotamers which occur at ca. ±120° (Figure 3). The syn-skew energy difference from the Fourier series is 0.59 kcal/mol and is again in accord with the most recent experimental estimate, 0.53 ± 0.42.[25b]

n-Pentane and *n*-hexane require more complex functions since they entail two and three internal rotations. This is handled using a Fourier series for each angle plus additional terms for nonbonded interactions between groups separated by more than three bonds (eq 3).[4] General parameters were developed for *n*-alkanes by

$$V(\phi,r) = \sum_i V(\phi_i) + \sum_{i<j}^{>1,4} (A_{CC}/r_{ij}^{12} - C_{CC}/r_{ij}^{6}) \qquad (3)$$

fitting to MM2 energies for 91 conformers of *n*-butane, *n*-pentane, *n*-hexane, and *n*-heptane. Since the Fourier coefficients and Lennard-Jones parameters were coupled in the least-squares analyses, it was finally decided to fix σ_{CC} at 4 Å. The resultant optimized Fourier coefficients are recorded in Table II and ϵ_{CC} = 0.0074 kcal/mol, so $A_{CC} = 4.973 \times 10^5$ kcal·Å^{12}/mol and C_{CC} = 121.4 kcal·Å^6/mol. A good fit to the 91 MM2 energies was obtained with a standard deviation of 0.24 kcal/mol. Some comparisons of results follow for a variety of conformers where the first number in parentheses is the MM2 value and the second is the prediction from eq 3 in kcal/mol: for *n*-pentane, tt (0.0, 0.0), tg (0.94, 0.85), g^+g^+ (1.62, 1.71), g^+g^- (3.23, 3.14); for *n*-hexane, ttt (0.0, 0.0), tgt (1.05, 0.92); and for *n*-heptane, tttt (0.0, 0.0), tttg (0.89, 0.86), g^+ttg^+ (1.75, 1.79), $g^+g^+tg^+$ (2.35, 2.78), tg^+tg^- (1.94, 1.80).

For all these rotational potentials, it is important to note that the MM2 results are for fully optimized, relaxed geometries, while the fit potentials utilize the fix standard bond lengths and angles in Table I. Thus, in fitting to eq 3 the MM2 nonbonded distances were not used, but rather those from the standard geometries. And, consequently, in using eq 3 with a given set of ϕ's, the nonbonded distances must be computed from geometries with the fixed bond lengths and angles.

It should also be noted that cyclopentane was taken to be planar for its simulation. Inclusion of pseudorotation in our simulation of liquid THF had a negligible effect on the resuls in comparison to the results for planar THF.[21b] The torsional motions for the five-membered rings are constrained by their limited flexibility.

(c) Monte Carlo Simulations. Standard procedures were used for the Monte Carlo simulations including Metropolis sampling and periodic boundary conditions.[4] Each full simulation involved an equilibration phase of 500K to 1000K configurations followed by averaging over 1000K configurations except for *n*-hexane in which case 1500K configurations were used for averaging. Each system consisted of 128 monomers in a cubic cell. The simulations were all carried out in the NPT ensemble with a pressure of 1 atm. Calculations for methane, ethane, propane, and *n*-butane were run at their boiling points and also at 25 °C for propane and *n*-butane. All other simulations were run at 25 °C. The ranges for the translations and rotations of the monomers and for the volume changes were adjusted to yield overall acceptance rates of ca. 40% for new configurations.

Umbrella sampling over chopped rotational barriers was used for the systems with internal rotations except for 1-butene owing to the low barriers in this case.[4] The ranges for the dihedral angle changes were ca. ±20° and were attempted for all dihedral angles of a monomer when it was moved. The monomers to be moved were chosen randomly, though the volume moves were attempted every 600 configurations.

The cutoff distance for the intermolecular interactions was a little less than half the average length of an edge of the periodic cube. It ranged from 9.5 Å for methane to 13 Å for benzene and 15 Å for *n*-hexane. The cutoff was based on roughly the center-of-mass separations. It is important to note that a correction was made during the simulations to the total energy for all interactions neglected beyond the cutoff. The computation was made in the usual way according to eq 4, where N is the number of

$$E_c = (N/2)\sum_i\sum_j \int_{r_c}^{\infty} 4\pi r^2 \rho g_{ij}(r) u_{ij}(r)\, dr \qquad (4)$$

monomers, i and j refer to the CH_n groups in a monomer, ρ is the number density (N/V), the radial distribution functions $g_{ij}(r)$ are taken to be 1 beyond the cutoff r_c, and $u_{ij}(r)$ is the Lennard-Jones potential for the i–j interaction. For the present systems, the cutoff correction accounts for 3–5% of the total energy which consists of the intermolecular and intramolecular terms in eq 5. The cutoff correction changes during the volume moves

$$E_T = E_i(l) + E_{intra}(l) \qquad E_T = \sum_{a<b} \epsilon_{ab} + E_c + \sum_a V(\phi_a, r_a) \qquad (5)$$

owing to the dependence on ρ and, therefore, directly affects their acceptance.

Results and Discussion

(a) Optimization of Lennard-Jones Parameters. The Lennard-Jones parameters for the intermolecular interactions were optimized in a sequential order with the aid of a series of relatively short (500K) Monte Carlo runs. The only exception is the parameters for methane which were adopted from the work of Verlet and Weis.[15]

The parameters for a saturated CH_2 group were determined first from simulations of liquid cyclopentane. The principal points for comparison with experiment were the liquid density and heat of vaporization. The CH_2 parameters were then used in simulations of *n*-butane at −0.5 °C and CH_3 group parameters were determined. When the CH_3 parameters were subsequently tried for isobutane, it became apparent that no reasonable CH parameters could be found without reducing the ϵ for CH_3. Consequently, four different methyl groups have been defined depending on the branching for the adjacent atom. The alternatives may be designated $CH_3(C_n)$ where n is the total number of nonhydrogen attachments for the adjacent atom. Then, isobutane and neopentane were simultaneously used to optimize the parameters for saturated CH, C, $CH_3(C_3)$, and $CH_3(C_4)$. The $CH_3(C_1)$ parameters were optimized separately in simulations of liquid ethane. Consistent trends were enforced, so the σ and ϵ parameters increase and decrease, respectively, as the branching (n) increases.

The parameters for vinylic groups were then determined from simulations of the isomeric butenes. The $CH(sp^2)$ parameters were obtained from *cis*-2-butene keeping the $CH_3(C_2)$ parameters fixed. The $CH_2(sp^2)$ parameters were determined from 1-butene and those for $C(sp^2)$ from isobutene. Finally, benzene was simulated to obtain parameters for an aromatic CH group. Uniform decreases of 0.05 Å for σ and increases of 0.022 to 0.055 kcal/mol for ϵ were found to be appropriate in going from saturated CH_n to vinylic CH_n. The optimized Lennard-Jones parameters are listed in Table III. After the optimizations, simulations were run for the remaining liquids, propane, *n*-pentane, isopentane, *n*-hexane, and *trans*-2-butene. The thermodynamic results con-

(24) Burkert, U.; Allinger, N. "Molecular Mechanics"; American Chemical Society: Washington, D.C., 1982.

(25) (a) Verma, A. L.; Murphy, W. F.; Bernstein, H. J. *J. Chem. Phys.* **1974**, *60*, 1540. (b) Van Hemelrijk, D.; Van den Enden, L.; Geise, H. J.; Sellers, H. L.; Schafer, L. *J. Am. Chem. Soc.* **1980**, *102*, 2189. (c) Maissara, M.; Cornut, J. C.; Devaure, J.; Lascombe, J. *Spectrosc. Int. J.* **1983**, *2*, 104.

Table III. Optimized Lennard-Jones Parameters for Hydrocarbons

group	example	σ (Å)	ϵ (kcal/mol)
CH_4	methane	3.730	0.294
CH_3 (C_1)	ethane	3.775	0.207
CH_3 (C_2)	*n*-butane	3.905	0.175
CH_3 (C_3)	isobutane	3.910	0.160
CH_3 (C_4)	neopentane	3.960	0.145
CH_2 (sp^3)	*n*-butane	3.905	0.118
CH_2 (sp^2)	1-butene	3.850	0.140
CH (sp^3)	isobutane	3.850	0.080
CH (sp^2)	2-butenes	3.800	0.115
CH (arom)	benzene	3.750	0.110
C (sp^3)	neopentane	3.800	0.050
C (sp^2)	isobutene	3.750	0.105

Table IV. Lennard-Jones Parameters from Earlier Work[a]

	GK[b]		TIPS[c]		UNICEPP[d]	
group	σ	ϵ	σ	ϵ	σ	ϵ
CH_3	3.47	0.23	3.86	0.18	3.79	0.18
CH_2	3.39	0.19	3.98	0.11	3.96	0.14
CH	3.30	0.14	4.25	0.05	4.23	0.13
C	3.21	0.20	4.44	0.03		
CH (arom)	3.39	0.22			3.74	0.12

[a] σ in Å, ϵ in kcal/mol. [b] Reference 11. [c] Reference 20. [d] Reference 9.

tinued to be in excellent accord with experiment and revealed the appropriate trends for isomeric series, as discussed in the next section. Therefore, no further adjustment of the parameters was made.

The trends in the Lennard-Jones parameters deserve further comment. In considering the first five entries in Table III, it is apparent that σ increases as the congestion at the adjacent carbon increases. A possible explanation may be related to the fact that although locating the interaction sites on the carbon nuclei is the convenient, logical choice, it may not be the optimum one. In fact, results of recent simulations of liquid ethane showed that improved accord with experimental X-ray data is obtained by using a longer "CC" bond for a two-site model.[16] This seems reasonable since the center of electron density for a CH_3 group is likely displaced along the threefold axis toward the hydrogens. Thus, to compensate for the use of normal CC bond lengths it is perhaps necessary for σ to increase owing to the increasing overlap of the proximate Lennard-Jones spheres in more crowded environments. Otherwise, the molecular volume becomes too small. On a percentage basis, the branching effect on ϵ for CH_3 groups is larger. This can be attributed to the diminished exposure of the methyl group and corresponding lower effective polarizability in a crowded environment.

There are two other general trends. The smaller σ and larger ϵ for vinylic rather than saturated CH_n groups are easily traced to the greater polarizability of the vinylic group from the π bond. The other trend is for decreasing σ and ϵ with decreasing n for CH_n. This is reasonable since the size and polarizability of a CH_n group should decrease with decreasing numbers of electrons. The same pattern is found in other potential functions such as those of Gelin and Karplus (GK)[11] and is also supported by the Slater–Kirkwood formula for the coefficient of the r^{-6} interactions.[26] In contrast, the TIPS[20] and UNICEPP[9] potentials have σ increasing along the series, though ϵ is decreasing as summarized in Table IV. On the basis of the present results, it is clear that the Gelin–Karplus parameters would yield liquids that are much too dense and low in energy. The TIPS and UNICEPP potentials are reasonable for *n*-alkanes,[17] but would fare poorly for branched system. The aromatic CH parameters from UNICEPP are fine and are also close to the values optimized recently by Claessens et al. (σ = 3.72, ϵ = 0.11).[19b]

(b) Thermodynamics. The thermodynamic results from the 17 full simulations are recorded in Tables V–VII. The computed volumes and densities are compared with the experimental values in Table V. The average statistical uncertainties (1σ) for the computed volumes and densities are ±0.5 Å^3 and ±0.002 g cm^{-3}. The values were obtained in the usual way from fluctuations in the averages for blocks of 50K configurations. The average error in comparison with experiment is 2.3%. The correct orders are also obtained for the three isomeric series, the butanes, pentanes, and butenes, given that the computed difference between 1-butene and isobutene is not statistically significant. The worst error (6.5%) occurs for propane at 25 °C which is 67° above its boiling point, though the volume at the boiling point is still 5.5% too large. However, the trend for the computed volumes for the *n*-alkanes is to become a little low with increasing chain length; e.g., the volume for *n*-hexane is 3.2% below the experimental figure.

As usual, the heat of vaporization is computed from eq 6, where

$$\Delta H_{vap} = E_{intra}(g) - (E_i(l) + E_{intra}(l)) + RT \qquad (6)$$

the intramolecular rotational energy for the gas may be obtained from a Boltzmann distribution for $V(\phi,r)$ for a monomer. This is easy to evaluate for cases with only one or two dihedral angles; however, for *n*-hexane, $E_{intra}(g)$ was determined from a Monte Carlo simulation for an isolated monomer. The chief approximation in eq 6 is that the sum of the kinetic and vibrational energies is the same for the gas and liquid. The computed and experimental heats of vaporization are compared in Table VI. The statistical uncertainties for the computed values average ±0.02 kcal/mol, while the average error in comparison with experiment is 2.1%. Again, the correct orders are obtained for the isomeric series even for the butenes where the differences between 1-butene and isobutene, and *cis*- and *trans*-2-butene, are slight.

The results for propane and *n*-butane are interesting in that they indicate that the optimum choice of Lennard-Jones parameters is undoubtedly temperature dependent. The ΔH_{vap} for propane is too low at the boiling point, but the result at 25 °C is correct, while the result for *n*-butane is correct at the boiling point and too high at 25 °C. The calculated values increase relative to experiment with increasing chain length for the *n*-alkanes reaching a 7% overestimate for *n*-hexane. It may be that a slightly smaller ϵ for CH_2 would be better, though it would clearly worsen the results for propane and *n*-butane at −0.5 °C.

The remaining thermodynamic quantities are the heat capacity (C_p), coefficient of thermal expansion (α), and isothermal compressibility (κ). They are calculated from standard fluctuation formulas and are well known to converge much more slowly than the energy or volume.[28] C_p for the liquid is estimated from the fluctuation in the intermolecular energy plus an intramolecular term taken as C_p for the ideal gas less R. The calculated values in Table VII are in good accord with the experimental data, though the substantial contribution from the ideal gas term must be noted. The computed C_p's are mostly a little low which can be attributed to insufficient convergence and imperfect separation of the intra- and intermolecular terms.

There is no doubt that κ and α certainly are not well converged in runs of the present length (ca. 1000K).[28] Their presence in Table VII is only to show that the computed values are in reasonable ranges. Experimental data for α along with the boiling points are provided for reference. Few experimental data are available for κ except for the *n*-alkanes, hexane to nonane. At 25 °C, κ varies from 175 × 10^{-6} to 124 × 10^{-6} atm^{-1} along this series.[29]

In summary, the computed densities and heats of vaporization are in excellent agreement with experiment for the 15 liquids. Though many of the liquids were involved in the parameter fitting, results of comparable quality were obtained subsequently for other

(26) Slater, J. C.; Kirkwood, J. G. *Phys. Rev.* **1931**, *37*, 682.

(27) (a) "Selected Values of Physical and Thermodyanmic Properties of Hydrocarbons and Related Compounds", American Petroleum Institute Research Project 44; Carnegie Press: Pittsburgh, 1953. (b) "Physical Constants of Hydrocarbons", ASTM Technical Publication No. 109A; American Society for Testing and Materials: Philadelphia, 1963.

(28) Jorgensen, W. L. *Chem. Phys. Lett.* **1982**, *92*, 405.

(29) Blinowska, A.; Brostow, W. *J. Chem. Thermodyn.* **1975**, *7*, 787. Eduljee, H. E.; Newitt, D. M.; Weale, K. E. *J. Chem. Soc.* **1951**, 3086.

Table V. Volumes and Densities for Hydrocarbon Liquids[a]

liquid	T (°C)	V	V(exptl)[b]	d	d(exptl)[b]
methane	−161.49	63.3	62.8	0.421	0.424
ethane	−88.63	91.7	91.5	0.545	0.546
propane	−42.07	132.9	126.0	0.551	0.581
propane	25.00	158.2	148.6	0.463	0.493
n-butane	−0.50	162.9	160.3	0.592	0.602
n-butane	25.00	168.7	168.4	0.572	0.573
isobutane	25.00	175.1	175.1	0.551	0.551
n-pentane	25.00	188.7	192.8	0.635	0.621
isopentane	25.00	190.9	194.9	0.628	0.615
neopentane	25.00	204.9	204.7	0.585	0.585
cyclopentane	25.00	157.9	157.3	0.738	0.740
n-hexane	25.00	211.5	218.5	0.677	0.655
1-butene	25.00	165.1	158.2	0.564	0.589
trans-2-butene	25.00	162.0	155.7	0.575	0.598
cis-2-butene	25.00	157.7	151.4	0.591	0.615
isobutene	25.00	164.4	158.4	0.567	0.588
benzene	25.00	148.9	148.4	0.871	0.874

[a] Volumes in Å^3 per molecule; densities in g cm^{-3}. [b] Experimental data from ref 27.

Table VI. Energetic Results for Hydrocarbon Liquids[a]

liquid	T (°C)	$-E_i$(l)	ΔH_{vap}	ΔH_{vap}(exptl)[b]
methane	−161.49	1.73	1.95	1.96
ethane	−88.63	3.15	3.52	3.52
propane	−42.07	3.72	4.18	4.49
propane	25.00	3.02	3.61	3.61
n-butane	−0.50	4.82	5.36	5.35
n-butane	25.00	4.58	5.18	5.04
isobutane	25.00	4.01	4.60	4.57
n-pentane	25.00	6.03	6.62	6.32
isopentane	25.00	5.59	6.17	5.88
neopentane	25.00	4.56	5.15	5.21
cyclopentane	25.00	6.15	6.74	6.82
n-hexane	25.00	7.47	8.07	7.54
1-butene	25.00	4.24	4.82	4.87
trans-2-butene	25.00	4.62	5.21	5.15
cis-2-butene	25.00	4.67	5.26	5.30
isobutene	25.00	4.27	4.86	4.92
benzene	25.00	7.68	8.27	8.09

[a] Energies and enthalpies in kcal/mol. [b] Experimental data from ref 27.

liquids such as *n*-pentane, isopentane, *n*-hexane, and *trans*-2-butene. The fluctuation properties, C_p, α, and κ were also computed; however, their slow convergence gives them little diagnostic value.

(c) Conformational Equilibria. The computed intramolecular rotational energies and conformer populations for the liquids and corresponding gases are listed in Tables VIII and IX. The average statistical uncertainties for E_{intra} and the conformer populations for the liquids are ±0.01 kcal/mol and ±0.5%. The principal conclusion from the results is that the condensed-phase environment has no significant effect on the conformational equilibria for any of these systems. This finding is in accord with earlier results for *n*-butane[17] and has been discussed at length previously.[4] It is also in agreement with recent Raman results for gaseous and liquid *n*-pentane.[25c]

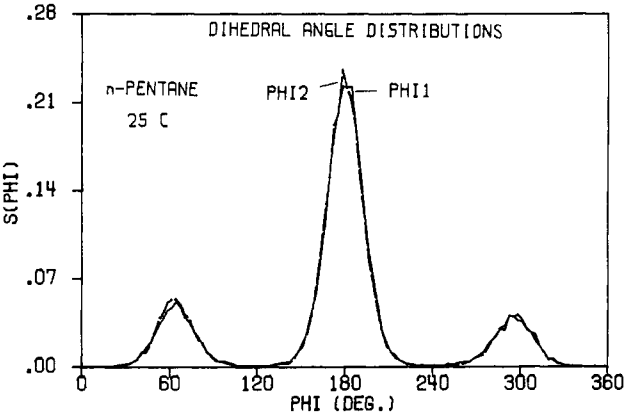

Figure 4. Computed population distributions for the dihedral angles about the C2C3 and C3C4 bonds in liquid *n*-pentane.

The full dihedral angle distributions, $s(\phi)$, are shown for *n*-butane, isopentane, and 1-butene at 25 °C in the top halves of Figures 1–3. The dashed curves are the ideal gas results for $s(\phi)$ derived from Boltzmann distributions for $V(\phi)$. Consistent with the data in Tables VIII and IX, the ideal gas and liquid distributions are almost identical. The near-perfect symmetry in the results for the liquids attests to the occurrence of balanced sampling. This is enhanced by the umbrella smapling techniques that were employed.[4]

Table VII. Boiling Points, Heat Capacities, Expansivities, and Compressibilities of Hydrocarbon Liquids[a]

liquid	T_b (°C)	T (°C)	C_p^{ig}	C_p^l (calcd)	C_p (exptl)	α (calcd)	α (exptl)	κ (calcd)
methane	−161.49	−161.49	6.0	9.5	13.2	245	349	172
ethane	−88.63	−88.63	8.6	14.5	17.6	190	231	156
propane	−42.07	−42.07	14.0	18.6	23.5	123	115	146
propane	−42.07	25.00	17.6	25.0	26.6	256	318	575
n-butane	−0.50	−0.50	21.9	27.8	31.8	119	176	186
n-butane	−0.50	25.00	23.3	29.3	33.4	117	309	208
isobutane	−11.73	25.00	23.1	29.8	33.8	164	227	297
n-pentane	36.07	25.00	28.7	39.0	39.9	124	160	178
isopentane	27.85	25.00	28.4	41.7	39.4	211	167	280
neopentane	9.50	25.00	29.1	36.2	40.8	148	200	273
cyclopentane	49.26	25.00	19.8	28.8	30.3	138	131	150
n-hexane	68.74	25.00	34.2	39.4	46.8	43	138	89
1-butene	−6.25	25.00	20.5	28.1	30.8	181	214	277
trans-2-butene	0.88	25.00	21.0	27.2	30.5	135	190	207
cis-2-butene	3.72	25.00	18.9	25.0	30.2	130	190	184
isobutene	−6.90	25.00	21.3	31.4	31.3	223	210	352
benzene	80.10	25.00	19.5	29.7	32.5	113	121	92

[a] C_p in cal/mol deg; α in deg^{-1} × 10^{-5}; κ in atm^{-1} × 10^{-6}. Experimental data from ref 27.

Table VIII. Calculated Intramolecular Rotational Energies (kcal/mol)

molecule	T (°C)	E_{intra}(g)	E_{intra}(l)
1-butene	25.0	0.43	0.44
n-butane	−0.5	0.56	0.56
n-butane	25.0	0.62	0.61
n-pentane	25.0	1.19	1.19
isopentane	25.0	0.43	0.44
n-hexane	25.0	1.73	1.72

Table IX. Calculated Conformer Populations

molecule	T (°C)	conformer	% gas	% liquid
1-butene	25.0	skew	81.2	79.1
		syn	18.8	20.9
n-butane	−0.5	t	71.1	71.9
		g	28.9	28.1
n-butane	25.0	t	68.2	69.3
		g	31.8	30.7
n-pentane	25.0	tt	46.5	47.0
		tg	47.1	45.7
		g^+g^+	5.4	6.0
		g^+g^-	1.0	1.3
isopentane	25.0	t	88.8	87.7
		g	11.2	12.3
n-hexane[a]	25.0	t_1	70.2	69.1
		g_1	29.8	30.9
		t_2	72.5	75.7
		g_2	27.5	24.3

[a] t_1 and t_2 refer to the trans populations for rotation about the C2C3 and C3C4 bonds. g_1 and g_2 are the corresponding gauche populations.

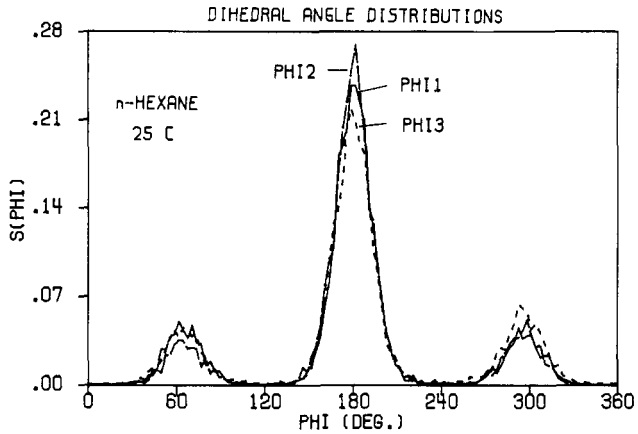

Figure 5. Computed population distributions for the dihedral angles about the C2C3 (ϕ_1), C3C4 (ϕ_2), and C4C5 (ϕ_3) bonds in liquid *n*-hexane.

The distributions for each dihedral angle in liquid *n*-pentane and *n*-hexane are presented in Figures 4 and 5. The results for both angles in *n*-pentane are essentially the same, as they should be by symmetry, though there is about 3% more g^+ than g^- for each. Such asymmetry is related to the limited system size, since it only requires an average of 2 of the 128 molecules to change from g^+ to g^- for each angle to attain perfect balance. For *n*-hexane, there is more statistical uncertainty in the distributions and conformer populations even though the averaging was 50% longer (1500K). This follows from the larger number of dihedral angles which caused the umbrella sampling to be more severe. Nevertheless, it appears that the central dihedral angle, ϕ_2, has a slightly higher trans population in both the liquid and gas (Table IX) than the outer angles. The more well-founded observation is that the trans population for each dihedal angle in the *n*-alkanes is about 70% at 25 °C.

(d) Energy Distributions. The energetic environments in the liquids were also monitored during the simulations. The distributions of total intermolecular bonding energies for the monomers are presented in Figure 6 for the alkanes at 25 °C and in Figure 7 for the alkenes and benzene. The monomers experience a range

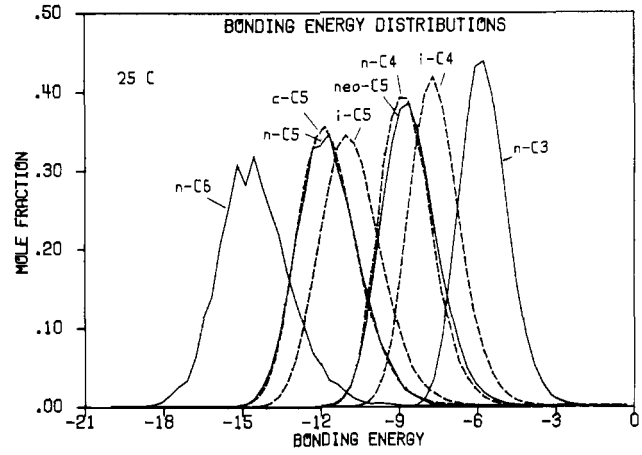

Figure 6. Distributions for the total intermolecular bonding energies (kcal/mol) of monomers in liquid alkanes at 25 °C. Units for the ordinate are mole fraction per kcal/mol.

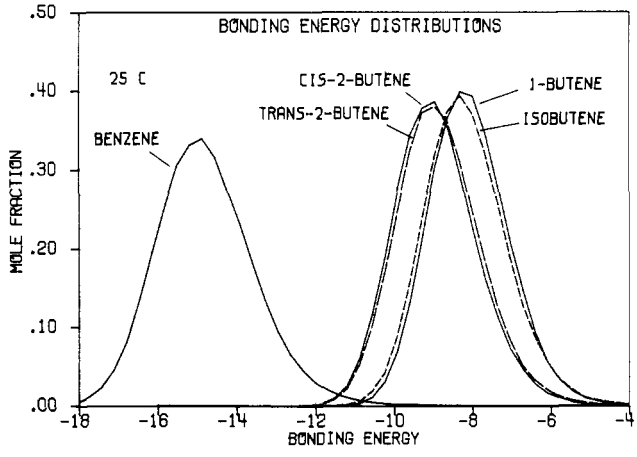

Figure 7. Distributions for the total intermolecular bonding energies (kcal/mol) of monomers in liquid alkenes and benzene at 25 °C. Units as in Figure 6.

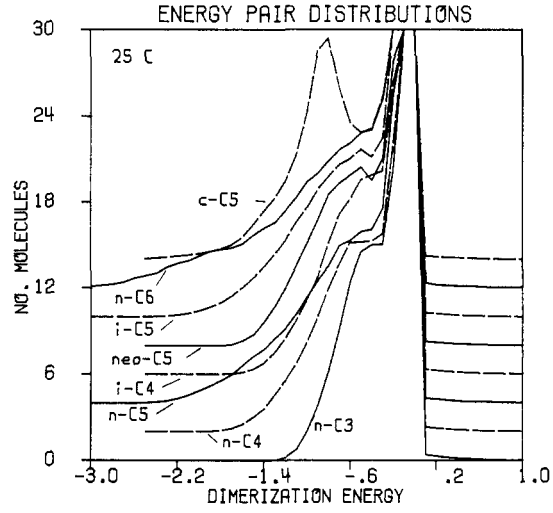

Figure 8. Distribution of dimerization energies (kcal/mol) for monomers in liquid alkanes at 25 °C. Units for the ordinate are number of molecules per kcal/mol. Successive liquids are offset 2 units along the ordinate for clarity.

of energetic environments covering from ca. 6 kcal/mol for propane to 9 kcal/mol for *n*-hexane and benzene. The larger molecules have the broader ranges since they have a wider range of individual interactions with neighbors. This is apparent in the distributions of dimerization energies for the monomers shown in Figures 8 and 9. It results from the fact that the variety of

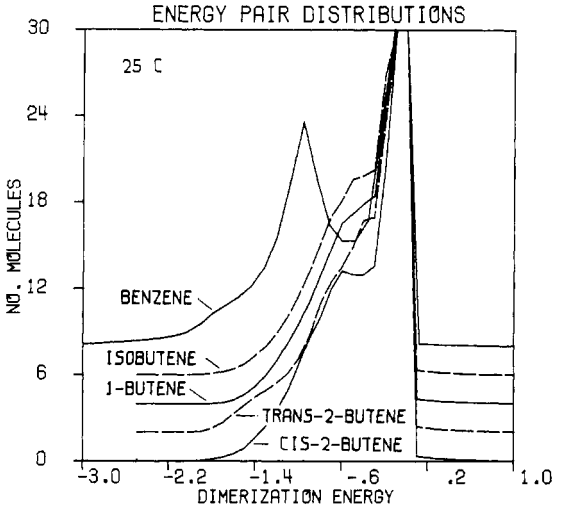

Figure 9. Distributions of dimerization energies (kcal/mol) for monomers in liquid alkenes and benzene at 25 °C. Successive liquids are offset 2 units along the ordinate for clarity. Units as in Figure 8.

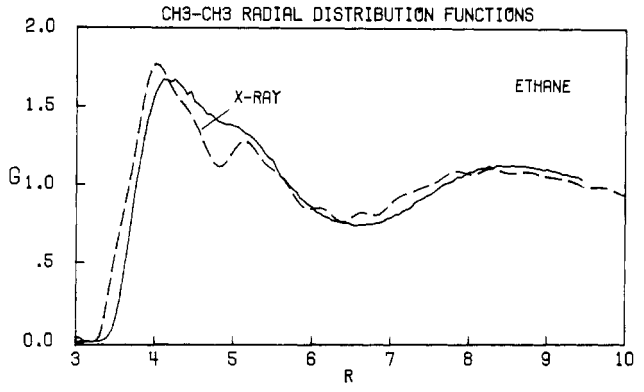

Figure 10. CH_3–CH_3 radial distribution functions for liquid ethane. Computed results (solid curve) are at −89 °C; experimental data (dashed curve) are at −92 °C. Distances are in ångströms thoughout.

geometric possibilities for contact with a neighbor increases with the size of the monomer.

Several other observations can be made from the distributions of dimerization energies. First, for these liquids there are few pair interactions more attractive than 2 kcal/mol, though the range does extend to about 3 kcal/mol for benzene and *n*-hexane. The favorable interactions with near neighbors yield the broad bands up to about −0.4 kcal/mol, while the many weak interactions with distant monomers are represented in the spikes near 0 kcal/mol. There are virtually no repulsive interactions in these systems, though they are common in polar liquids and at higher densities.[17b] Another point is that the low-energy bands in these distributions may be integrated to obtain estimates of the number of near neighbors. The results are sensitive to the integration limit; the break point between the low-energy band and the bulk spike shifts from about −0.2 kcal/mol for propane to roughly −0.5 kcal/mol for benzene, *n*-hexane, and cyclopentane. Integration to the break points yields coordination numbers of 10–12 in each case.

A final, outstanding feature in the distributions of dimerization energies is the sharp maxima in the low-energy range for the two cyclic molecules, benzene and cyclopentane. In fact, the same pattern is accentuated for methane, represented here as the simplest Lennard-Jones liquid. Thus, the shell of nearest neighbors around a spherical or disk-like monomer is more clearly defined owing to the possibility of uniform packing, as discussed further in the next section. Apparently, the packing is effectively not as uniform for neopentane since its dimerization energy distribution only has a weak maximum at about −0.5 kcal/mol.

(e) Structure. All of the unique carbon–carbon radial distribution functions (rdf's) were determined during the simulations. There are too many to report all of them here, so the focus will

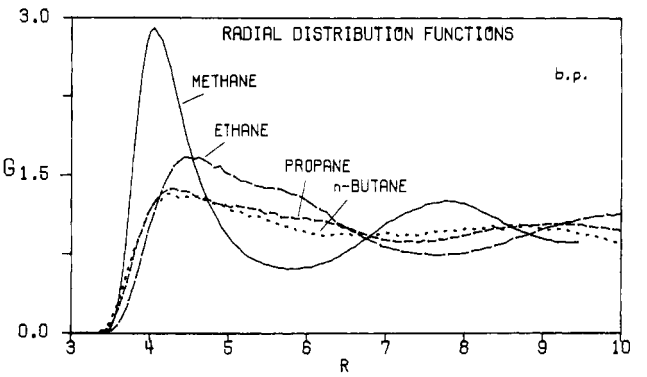

Figure 11. Computed C–C rdf for liquid methane and CH_3–CH_3 rdf's for liquid ethane, propane, and *n*-butane at their boiling points. Effect of chain length on end group rdf's is illustrated.

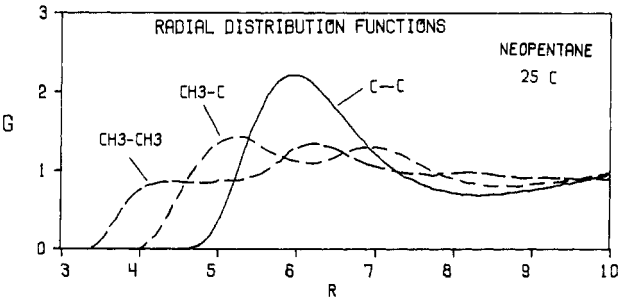

Figure 12. Computed rdf's for liquid neopentane at 25 °C.

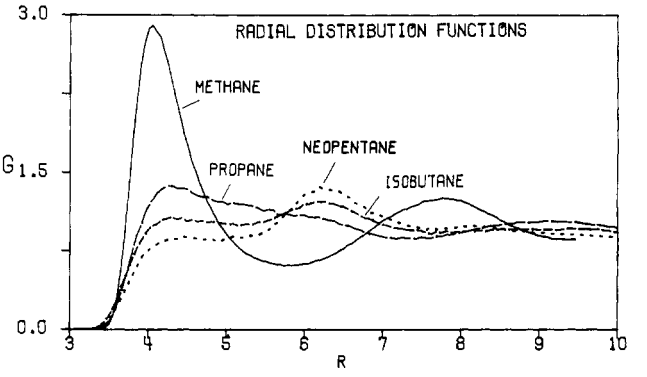

Figure 13. Computed C–C rdf for liquid methane and CH_3–CH_3 rdf's for liquid propane, isobutane, and neopentane. Results for methane and propane are at their boiling points and for isobutane and neopentane at 25 °C. Effect of branching on end group rdf's is illustrated.

be on trends as a function of chain length and branching. However, first some comparisons with experimental data can be made.

Among the present liquids, radial distribution functions have been obtained by X-ray diffraction for methane, ethane, neopentane, and benzene.[30–33] The experimental CC rdf for liquid ethane at −92 °C is compared with the simulation results at −89 °C in Figure 10. This illustrates the typical level of accord between theory and experiment for these systems. Overall, the agreement for peak heights and positions is good, though the experimental curves often show somewhat greater structure. For methane, the computed CC rdf in Figure 11 at −161 °C also agrees well with the experimental result at −181 °C.[30] Experimentally, the locations and heights of the first two peaks are 4.1 Å, 2.7 and 7.6 Å, 1.3, while the simulation yielded 4.1 Å, 2.9 and 7.8 Å, 1.3.

(30) Habenschuss, A.; Johnson, E.; Narten, A. H. *J. Chem. Phys.* **1981**, *74*, 5234.
(31) Sandler, S. I.; Lombardo, M. G.; Wong, D. S.-H.; Habenschuss, A.; Narten, A. H. *J. Chem. Phys.* **1982**, *77*, 2144.
(32) Narten, A. H. *J Chem. Phys.* **1979**, *70*, 299. Narten, A. H.; Sandler, S. I.; Rensi, T. A. *Discuss. Faraday Soc.* **1978**, *66*, 39.
(33) Narten, A. H. *J. Chem. Phys.* **1977**, *67*, 2102; **1968**, *48*, 1630.

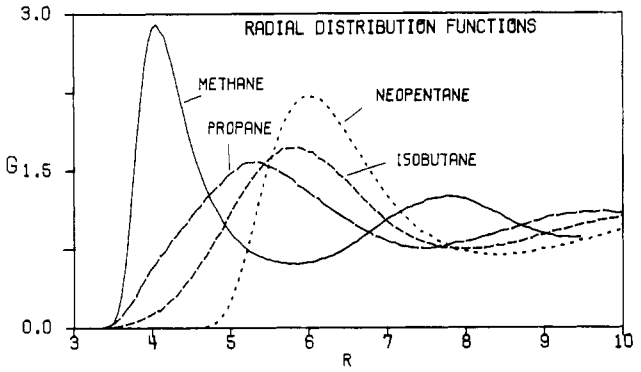

Figure 14. Computed central group–central group rdf's for liquid methane (C–C), propane (CH_2–CH_2), isobutane (CH–CH), and neopentane (C–C). Results for methane and propane are at their boiling points and for isobutane and neopentane at 25 °C. Effect of branching on central group rdf's is illustrated.

From both a structural and thermodynamic standpoint, a Lennard-Jones description for methane appears to be reasonable.

The three CC rdf's for neopentane calculated at 25 °C are shown in Figure 12. Only a combined rdf has been obtained experimentally which is dominated by the methyl–methyl contribution.[32] The combined curve at 25 °C begins at 3.5 Å and has a shoulder near 4 Å, the major peak at 6.1 Å, and a second peak at 11.2 Å.[32] The shoulder can be assigned to the first peak in Figure 12 for the methyl–methyl contacts, while the peak at 6.1 Å coincides with the principal maximum for both the C-H_3–CH_3 and C–C rdf's in Figure 12. Theoretical and experimental results for benzene have been compared recently by Claessens et al.[19b] Their LJ6 potential and its results are virtually identical with ours. The computed CC rdf has a shoulder at 5 Å and a low (1.2) peak at 6 Å. The same features are found in the experimental data which also reveal some additional ripples between 4 and 5 Å.[33]

The effect of increasing chain length on the CH_3–CH_3 rdf's is illustrated in Figure 11 for the four smallest *n*-alkanes at their boiling points. The shielding by the rest of the molecule causes the first peak to be substantially suppressed in proceeding from methane to ethane to propane. The effect levels off between propane and *n*-butane. The difference between these two and *n*-pentane and *n*-hexane is also small; there is a slight lowering of the peaks at 4 and 9 Å, and a slight raising of the minimum at 7.5 Å. That is, the methyl–methyl rdf is becoming essentially structureless with increasing chain length. The pronounced structure for methane is clearly due to its spherical shape. In fact,

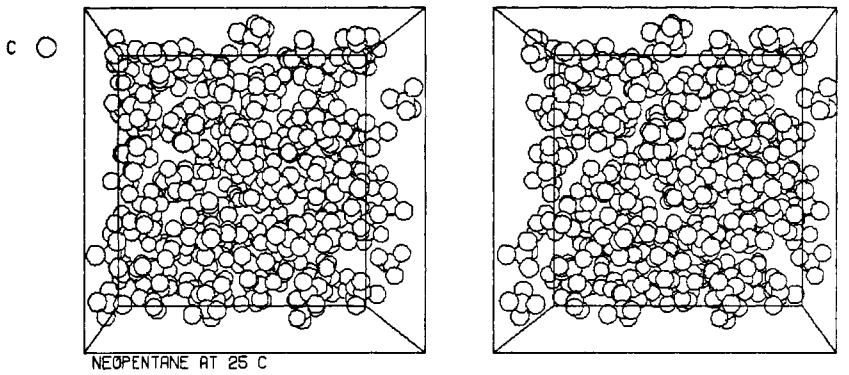

Figure 15. Stereoplot of a configuration from the simulation of liquid neopentane at 25 °C.

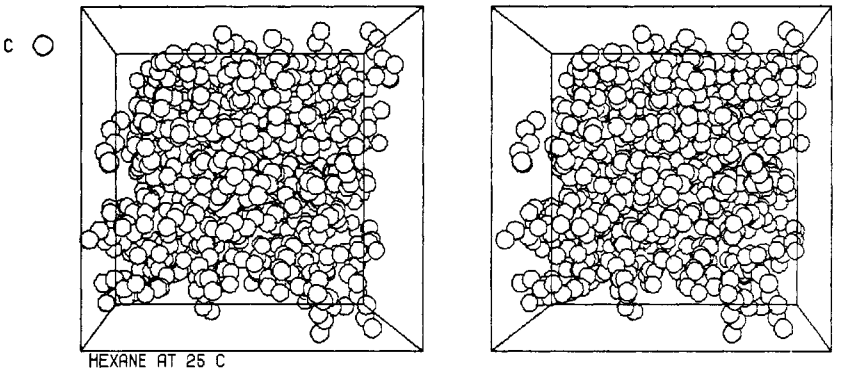

Figure 16. Stereoplot of a configuration from the simulation of liquid *n*-hexane at 25 °C.

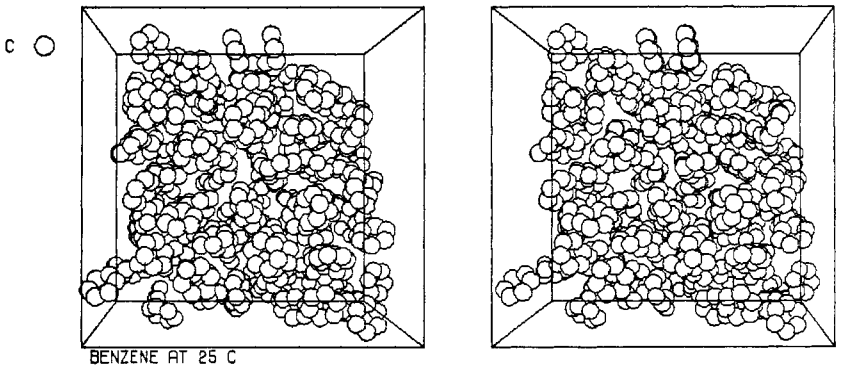

Figure 17. Stereoplot of a configuration from the simulation of liquid benzene at 25 °C.

the first peak integrates to 12 neighbors which corresponds to close packing of spheres. The rapid departure from spherical symmetry with increasing chain length is reflected in Figure 11. It also shows the shielding effect of the rest of the molecule is nearly complete once propane is reached. This is consistent with the predominance of trans bonds in the higher *n*-alkanes. It may also be noted that the CH_2–CH_2 rdf's for the methylene group next to methyl for *n*-butane, *n*-pentane, and *n*-hexane are also similiar at 25 °C and show little structure besides a weak (1.3) maximum near 4.5 Å.[17]

The effect of adjacent branching on the CH_3–CH_3 rdf's is shown in Figure 13. The results for methane and propane are at their boiling points and for isobutane and neopentane at 25 °C. The increased shielding of the terminal group by a bulkier adjacent group is obvious in the reduction of the first peak at 4.1 Å. However, there is progressive growth of a peak near 6.2 Å. For isobutane and neopentane, the latter feature corresponds to the distances to the other methyl groups of the neighbor as illustrated in II. Clearly, not all contacts are as in II; otherwise the peak at 6.2 Å would be much larger.

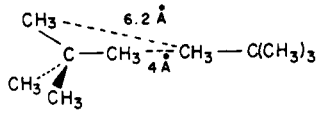

II

Another progression that can be illustrated is for the central group–central group rdf's for methane, propane, isobutane, and neopentane. Figure 14 illustrates the obvious fact that as the size of the molecule grows, the first peak in the central group–central group rdf moves to larger separation. More interesting, as roughly spherical symmetry is restored in progressing from propane to isobutane to neopentane, the first peak grows back. In fact, integrating the first peak in the CC rdf for neopentane yields 12 neighbors out to the minimum at 8.4 Å. Thus, the centers of the neopentanes are distributed in a spherical sense, though the local environment for the methyl groups is asymmetric (Figure 12).

In closing this section on structure, a few stereoplots of configurations from the simulations may be presented. Neopentane, *n*-hexane, and benzene were selected in Figures 15–17 owing to the diversity of the structures of the monomers. It should be noted that: (1) the 128 monomers are present in each case, (2) the edges of the cube in the plots are shown for perspective and are actually a little outside the edges of the periodic cube in the simulations, and (3) the plots only show one of one million configurations. There is clearly little global order in the liquids. The parallel alignment of all trans monomers in solid *n*-hexane is replaced by monomers that mostly have at least one gauche bond and that point in all directions. Liquid benzene is also disordered, though edge-to-face orientations are common and there is the interesting face-to-face pair at the top of the figure. The orientational structure for benzene and the alkenes would undoubtedly be affected by the addition of appropriate multipole interactions to the potential functions. Though the effects may be hard to detect for the liquids, incorrect energetic ordering of alternate crystalline forms may be anticipated with the simple Lennard-Jones description.[19b]

Conclusion

An extensive study of hydrocarbon liquids was undertaken to optimize potential functions for describing interactions between monomers in the fluids. The derived parameters form a basis for the development of an extensive set of optimized potential functions for liquid simulations that may be applied to organic and biochemical systems. The thermodynamic and structural results from Monte Carlo simulations were shown to be in good accord with available experimental thermodynamic and structural data. In particular, the errors in the computed heats of vaporization and densities are 2% and trends in these quantities for isomeric series are reproduced. Conformational results were also obtained for five liquids and showed no condensed-phase effects on the conformer populations. In addition, structural analyses were performed and revealed understandable trends as a function of chain length and branching of the monomers.

Acknowledgment. Gratitude is expressed to the National Science Foundation and National Institutes of Health for support of this work. Dr. Phillip Cheeseman kindly provided the program for making the stereoplots. Discussions with Dr. J. Chandrasekhar were helpful. The authors are also grateful to Drs. A. Habenschuss and A. H. Narten for tabular results of their X-ray studies.

Registry No. Methane, 74-82-8; ethane, 74-84-0; propane, 74-98-6; *n*-butane, 106-97-8; isobutane, 75-28-5; *n*-pentane, 109-66-0; isopentane, 78-78-4; neopentane, 463-82-1; cyclopentane, 287-92-3; *n*-hexane, 110-54-3; 1-butene, 106-98-9; *trans*-2-butene, 624-64-6; *cis*-2-butene, 590-18-1; isobutene, 115-11-7; benzene, 71-43-2.